

HEAT TRANSFER ON MAGNETOHYDRODYNAMIC STAGNATION POINT FLOW THROUGH A POROUS SHRINKING/STRETCHING SHEET A Numerical Study

by

**Munawwar A. ABBAS^{a*}, Muhammad M. BHATTI^b,
and Mohammad M. RASHIDI^c**

^a Department of Mathematics, University of Baltistan, Skardu, Gilgit-Baltistan, Pakistan

^b College of Mathematics and System Science, Shandong University of Science and Technology,
Qingdao, Shandong, China

^c Shanghai Key Lab of Vehicle Aerodynamics and Vehicle Thermal Management Systems,
Tongji University, Shanghai, China

Original scientific paper

<https://doi.org/10.2298/TSCI181025067A>

This article examines the numerical study of heat transfer analysis on MHD stagnation point flow past a permeable shrinking/stretching sheet through a porous media. The governing equations have been reduced to the ODE by utilizing similarity variables. The obtained highly non-linear coupled differential equations have been solved by implementing a numerical scheme labeled as successive linearization method. The influences for the pertinent parameters on velocity profile and temperature profile is debated and demonstrated graphically. Numerical comparisons in some special cases have been brought along the prevailing literature, and it is noticed that the current outcomes are in good concord.

Key words: heat transfer, MHD, porous medium, successive linearization method

Introduction

The analysis of stagnation point flow alongside heat transfer has gained a lot of interest due to its immense area of applications in many industrial developments. These applications involve continuous casting, fibers spinning, drying and cooling of papers, textiles, glass blowing, and aerodynamics extrusion of plastic sheet, *etc.* A stagnation point flow depicts the movement of the fluid very close to the stagnation region where the fluid moves towards a solid body. The stagnation region confronts the largest rate of mass deposition, heat transfer, and highest pressure. Himenz [1] earlier described the 2-D stagnation point flow. Later, different authors analyzed the behavior of stagnation point flow in various geometrical aspects [2-9].

The transport of fluid through a porous medium has also very much important in geothermal and petroleum industry. Various examples of porous media can be found in granular insulation, fiber insulation, cores of nuclear reactors, density electric machines, metallurgy, thermal insulation of buildings, geophysical systems, underground disposal of nuclear/non-nuclear waste, electrochemistry, cooling of various electronic devices and food processing. Rosali *et al.* [10] discussed unsteady mixed convection boundary-layer flow towards a stagnation point over a heated vertical surface embedded in a porous media while in another investigation they

* Corresponding authors, e-mail: munawer.abbas@uobs.edu.pk; muhammad09@shu.edu.cn

reported stagnation-point flow and heat transfer through the porous medium [11]. Some more studies related to the porous stretching sheet can be found from references [12-16].

The MHD play a symbolic role in boundary-layer flow past a stretching surface to control the heat transfer and momentum. The MHD is also applicable in the process of non-metallic inclusion and purification process of molten metals. Various professional methods regarding polymers require the cooling of continuous filaments and strips by drawing them from moving the fluid. Due to such significant importance of magnetic force over a stretching sheet, several authors investigated different fluid models with MHD effects. For instance, El-Aziz [17] examined the stagnation point flow over the shrinking/stretching surface under the influence of heat transfer, magnetic field and variable surface heat flux. Maabood *et al.* [18] studied the linear viscoelastic fluid model on stagnation point flow on a stretching/shrinking plate and the stagnation point flow with heat transfer and MHD on a stretched surface with the impact of chemical reaction and transpiration. Moreover, distinct investigators examined the stagnation point flow along various geometrical aspects can be found from the references [19-25].

This investigation aims to analyze heat transfer impact of MHD stagnation point flow over a permeable shrinking/stretching surface through a porous media. The numerical scheme we adopted for current study is robust and accurate. This numerical method is so powerful to get the solution for the highly coupled non-linear PDE. Further with the help of this method the governing non-linear resulting differential equation and boundary condition transformed into the iterative scheme. The iterative scheme can be further solved with the help of Chebyshev method.

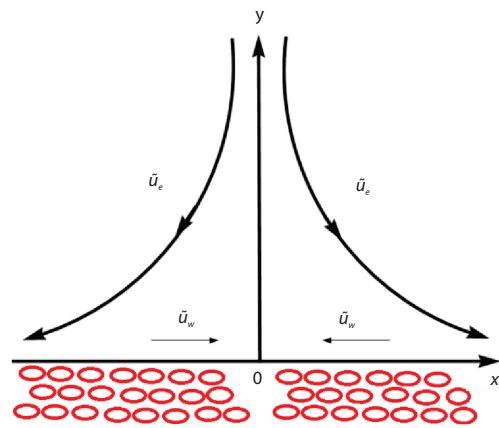


Figure 1. Geometry of the problem

Mathematical formulation

Suppose the steady 2-D incompressible, irrotational, MHD viscous fluid-flow in the region of stagnation point past a stretching/shrinking porous surface concurring along the plane at $y=0$. The electrically conducting fluid via extraneous magnetic field B_0 exercised to it taking the induced magnetic field to be neglected.

The Cartesian co-ordinate system has been taken in such way that \bar{x} -axis is considered along with the plate, \bar{y} -axis is regarded normal to it, see fig. 1. The flow being restricted to $\bar{y} > 0$, the governing equations of the present flow can be expressed:

$$\frac{\partial \bar{u}}{\partial x} + \frac{\partial \bar{v}}{\partial y} = 0 \quad (1)$$

$$\rho \left(\bar{u} \frac{\partial \bar{u}}{\partial x} + \bar{v} \frac{\partial \bar{u}}{\partial y} \right) = -\frac{\partial \bar{p}}{\partial x} + \mu \frac{\partial^2 \bar{u}}{\partial y^2} + \bar{u}_e \frac{d\bar{u}_e}{dx} + \left(\sigma \bar{B}_0^2 + \frac{\mu}{k} \right) (\bar{u}_e - \bar{u}) \quad (2)$$

$$\bar{u} \frac{\partial \bar{T}}{\partial x} + \bar{v} \frac{\partial \bar{T}}{\partial y} = \alpha \frac{\partial^2 \bar{T}}{\partial y^2} + \frac{v}{c_p} \left(\frac{\partial \bar{u}}{\partial y} \right)^2 + \frac{\sigma \bar{B}_0^2}{\rho c_p} (\bar{u}_e - \bar{u})^2 \quad (3)$$

The relevant boundary conditions:

$$\bar{u} = \bar{u}_w(\bar{x}), \quad \bar{v} = \bar{v}_w(\bar{x}), \quad \bar{T} = \bar{T}_w(\bar{x}), \quad \bar{y} = 0, \quad \bar{u} \rightarrow \bar{u}_e(\bar{x}), \quad \bar{T} \rightarrow \bar{T}_\infty, \quad \bar{y} \rightarrow \infty \quad (4)$$

In the aforementioned equations, $\bar{u}_e = \bar{u}_w = a\bar{x}$, $\bar{T}_w = b\bar{x}^2 + \bar{T}_\infty$. The similarity variables are presented:

$$\zeta = \sqrt{\frac{a}{\nu}} \bar{y}, \quad \bar{u} = a\bar{x}f'(\zeta), \quad \bar{v}_w = -\sqrt{a\nu}\beta, \quad \bar{v} = -\sqrt{a\nu}f(\zeta), \quad \theta(\zeta) = \frac{\bar{T} - \bar{T}_\infty}{\bar{T}_w - \bar{T}_\infty} \quad (5)$$

Substituting eq. (5) into eqs. (1)-(4), we obtained:

$$f''' - [f' + M + K]f' + 1 + M + K + ff'' = 0 \quad (6)$$

$$\theta'' - [2f'\theta - EcM(f' - 1)^2 - Ec f''^2 - f\theta']Pr = 0 \quad (7)$$

where prime denotes differentiation with respect to ζ . The corresponding boundary conditions takes the new form:

$$\theta(0) = 1, \quad f'(0) = \alpha, \quad f(0) = \beta, \quad \theta(\infty) = 0, \quad f'(\infty) = 1 \quad (8)$$

The modelling for skin friction coefficient and local Nusselt number in dimensionless mode can be defined:

$$\sqrt{Re_x} C_f = f''(0), \quad \frac{Nu_x}{\sqrt{Re_x}} = -\theta'(0) \quad (9)$$

where

$$Re_x = \frac{\bar{u}_e \bar{x}}{\nu}, \quad K = \frac{\nu}{a\bar{k}}, \quad Ec = \frac{\bar{u}_w(\bar{x})^2}{\rho(\bar{T}_w - \bar{T}_\infty)c_p}, \quad M = \frac{\sigma B_0^2}{\rho a}, \quad Pr = \frac{\nu}{a\bar{\alpha}} \quad (10)$$

In the aforementioned equation, the parameter Re_x is the Reynolds number, K – the dimensionless porosity parameter, Ec – the Eckart number, M – the Hartman number, and Pr – the Prandtl number.

Numerical method

We employ the successive linearization method (SLM) to eq. (6) along with eq. (7), by implementing [26, 27]:

$$f(\zeta) = f_n(\zeta) + \sum_{m=0}^{n-1} f_m(\zeta), \quad (n = 1, 2, 3, \dots) \quad (11)$$

where f_n are unknown functions which are obtained by iteratively solving the linearized version of the governing equation and presuming that $f_n(0 \leq m \leq n - 1)$ are obtained from early iterations. The algorithm commences with an initial approximation $f_0(\zeta)$ that obey the given boundary conditions in eq. (7) according to SLM. The suitable initial guess for the governing flow problem:

$$f_0(\zeta) = \frac{\zeta \exp[\zeta] + \alpha \exp[\zeta] + \beta \exp[\zeta] - \alpha - \exp[\zeta] + 1}{\exp[\zeta]} \quad (12)$$

For generality, expressed the equations:

$$\ell_L + \ell_n = 0 \quad (13)$$

where

$$\ell_L = f''' \quad (14)$$

and

$$\ell_n = -[f' + M + K]f' + 1 + M + K + ff'' \quad (15)$$

where ℓ_L and ℓ_n are the linear and non-linear terms of eq. (6). By replacing eq. (11) into eq. (6)-(8) and neglecting the non-linear terms:

$$f_n''' + \Gamma_{0,n-1}f_n'' + \Gamma_{1,n-1}f_n' + \Gamma_{2,n-1}f_n = \mathfrak{R}_{n-1} \quad (16)$$

and boundary condition are:

$$f_n(0) = 0, \quad f_n'(0) = 0, \quad f_n'(\infty) = 0 \quad (17)$$

To solve eq. (13) a numerical scheme known as Chebyshev spectral collocation (CSC) method is employed. The physical region $[0, \infty)$ is truncated to $[0, \Theta]$ we can deal Θ to be enough large. The said region is farther reconstructed in to $[-1, 1]$ by below conversion:

$$\Omega = 2\Theta^{-1}\zeta - 1 \quad (18)$$

The Gause-Lobatto collocation points for defining the nodes in $[-1, 1]$ have been implemented:

$$\Omega_M = \frac{1}{\sec\left(\frac{\pi M}{\gamma}\right)}, \quad (M = 0, 1, \dots, \gamma) \quad (19)$$

with $(\gamma + 1)$ number of collocation points. The CSC method planted on the conception of differentiation matrix \mathbf{D} . This \mathbf{D} corresponds a vector of the function values $\mathbf{G}_n = [f(\Omega_0), \dots, f(\Omega_M)]^T$, the collocation points for a vector \mathbf{G} is given:

$$\mathbf{G} = \sum_{l=0}^M \mathbf{D}_{lM} f(\Omega_l) = \mathbf{D}\mathbf{G} \quad (20)$$

theth \mathbb{N}^{th} order differentiation for $f(\Omega)$ can be described:

$$f^{(l)}(\Omega) = \mathbf{D}\mathbf{G} \quad (21)$$

The entries of matrix \mathbf{D} can be calculated via the scheme offered by Bhatti *et al.* [26, 27]. By employing the spectral method along derivative matrices on-linearized eqs. (16) and (15):

$$\Gamma_{n-1}\mathbf{G}_n = \mathfrak{R}_{n-1} \quad (22)$$

the boundary conditions take the form:

$$f_n(\Omega_M) = 0, \quad \sum_{l=0}^M \mathbf{D}_{lM} f_n(\Omega_M) = 0, \quad \sum_{l=0}^M \mathbf{D}_{0l} f_n(\Omega_M) = 0, \quad \sum_{l=0}^M \mathbf{D}_{0l}^2 f_n(\Omega_M) = 0 \quad (23)$$

where as:

$$\Gamma_{n-1} = \mathbf{D}^3 + \Gamma_{0,n-1}\mathbf{D}^2 + \Gamma_{1,n-1}\mathbf{D} + \Gamma_{2,n-1} \quad (24)$$

where $\Gamma_{\delta,n-1}$ ($\delta = 0, 1, \dots$) are $(M + 1) \times (M + 1)$ diagonal matrices along $\Gamma_{\delta,n-1}(\Omega_M)$ at the principal diagonal:

$$\mathbf{G}_n = f_n(\Omega_M), \quad \mathfrak{R}_n = \mathfrak{R}_n(\Omega_M) \quad (25)$$

Operating eq. (20) on the linear matrix system in eq. (20) provides the solutions for f_n by applying iterative scheme for solving the system in eq. (21) and achieved the solution for $f(\zeta)$ from eq. (20). Equation (6) can be resolved by employing Chebyshev pseudo spectral method directly since it is linear equation, that become:

$$BH = \mathring{A} \tag{26}$$

with boundary conditions:

$$\theta(\Omega_M) = 1, \theta(\Omega_0) = 0 \tag{27}$$

and

$$\mathbf{B} = \mathbf{D}^2 - [2f'\theta - EcM(f-1)^2 - Ecf'^2 - f\mathbf{D}]Pr \tag{28}$$

where $\mathbf{H} = \theta(\Omega_M)$, \mathring{A} is a vector of zeros, and all vectors in eq. (24) are changed to diagonal matrix. We implement the boundary conditions eq. (23) over the first and last rows of \mathbf{B} and \mathbf{S} appropriately.

Results and discussion

This portion describes all the outcomes in the form of tables and graphs of the related parametric quantities for velocity and temperature profile against stretching parameter, Hartmann number, porosity parameter, suction/injection parameter, Prandtl and Eckert numbers. For this purpose, figs. 2-7 have been plotted. Numerical comparability has been brought through tab. 1 with the existing literature of Yasin *et al.* [21], Aman *et al.* [20], and Wang [28] by taking $M = 0, K = 0$ for shrinking case ($\alpha > 0$). It is found that the current outcomes are in excellent agreement with the existing literature which assures the validity of our present flow problem. Table 2 shows the numerical values of Nusselt number for various values all the emerging parameters.

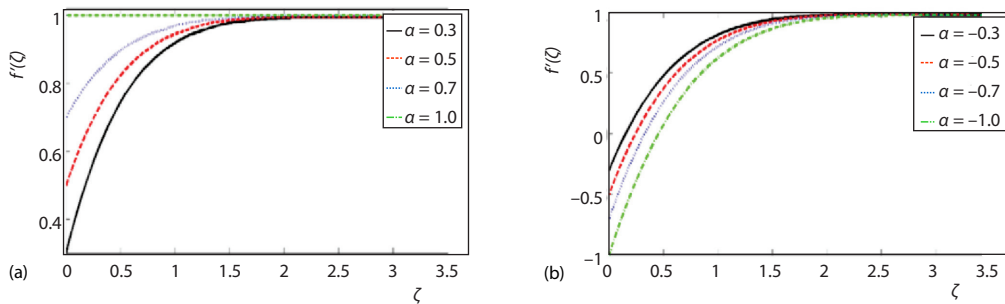


Figure 2. Effect of stretching parameter ($\alpha > 0$) on f' and ($\alpha < 0$) on f'

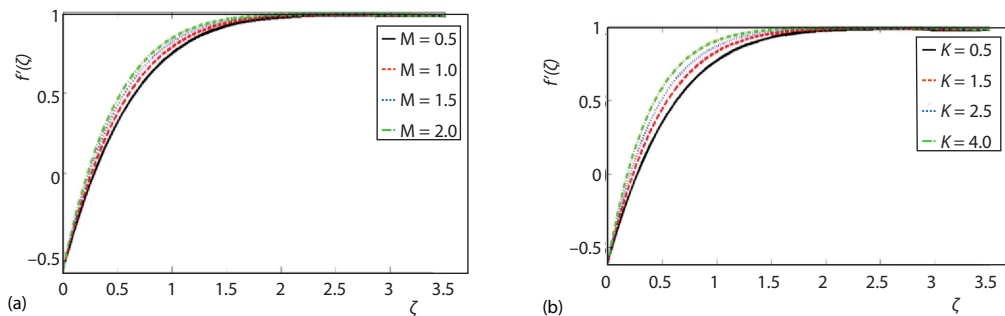


Figure 3. Effect of stretching parameter M on f' and κ on f'

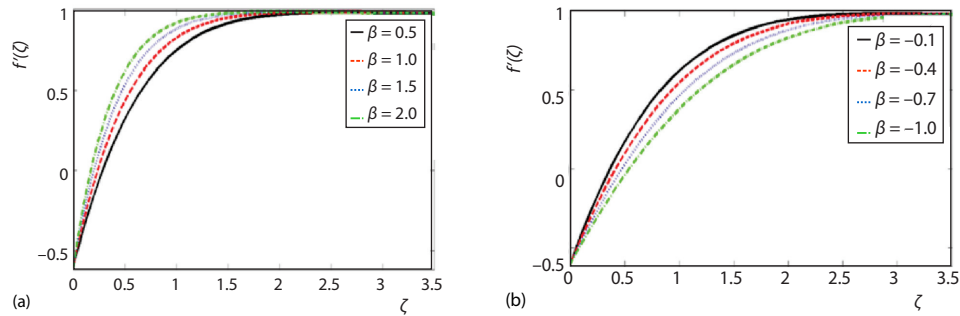


Figure 4. Effect of stretching parameter ($\beta > 0$) on f' and ($\beta < 0$) on f'

Figures 2-4 are conducted to explain the behavior of velocity profile for related parameters. Figure 2(a) depicts the behavior of stretching parameter ($\alpha > 0$) on velocity. We noticed from this figure that by raising the stretching parameter increases then the velocity distribution, which shows that the boundary-layer thickness increases. On the other hand, a reverse trend of velocity is observed when the stretching parameter decreases ($\alpha < 0$) in fig. 2(b). Which indicates that the boundary-layer thickness layer decreases. Figures 3(a) and 3(b) conceives the behavior of velocity profile with the variation of M and K , respectively. It concludes from these figures that with the increase in M and K velocity profile enhances. Physical point view, with the increment in magnetic parameter resistance between the fluid particles produced and as results, thermal boundary-layer becomes thicker. It is evident from fig. 4(a) that for positive values ($\beta > 0$) of suction/injection parameter, the velocity profile develops but reverse phenomena is indicated for negative values of suction/injection parameter ($\beta < 0$) as shown in fig. 4(b). This trend of velocity agrees the general physical behavior of suction and injection parameter

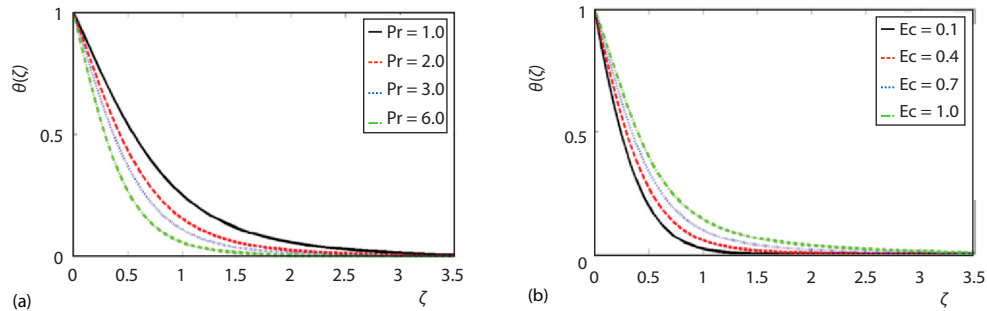


Figure 5. Effect of stretching parameter Pr on θ and stretching parameter Ec on θ

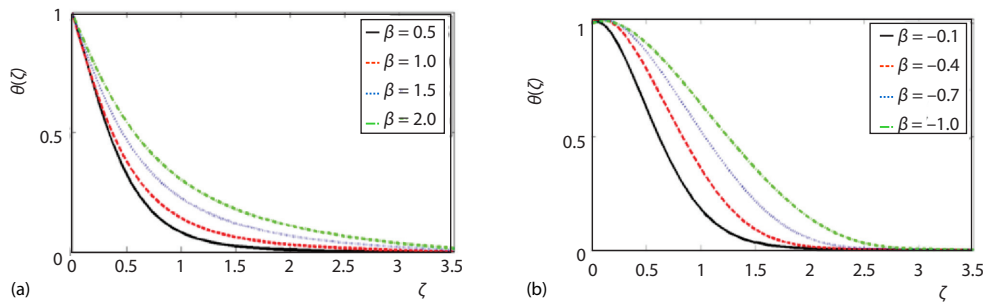


Figure 6. Effect of stretching parameter ($\beta > 0$) on θ and ($\beta < 0$) on θ

Table 1. Numerical comparison with the existing literature with different values of $f''(0)$ for shrinking case ($\alpha < 0$)

| | Present results | [21] | [22] | [28] |
|----------|-----------------|--------------|--------------|--------------|
| α | M = 0, K = 0 | M = 0, K = 0 | M = 0, K = 0 | M = 0, K = 0 |
| -0.25 | 1.4023 | 1.4022 | 1.4022 | 1.4022 |
| -0.50 | 1.4957 | 1.4956 | 1.4957 | 1.4956 |
| -1.00 | 1.3289 | 1.3288 | 1.3288 | 1.3288 |
| -1.10 | 1.1868 | 1.1866 | | |
| -1.15 | 1.0823 | 1.0822 | 1.0822 | 1.0822 |
| -1.18 | 1.0004 | 1.0004 | 1.0004 | |
| -1.20 | 0.9324 | 0.9324 | | |

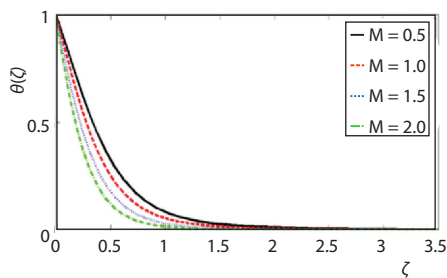


Figure 7. Effect of stretching parameter M on θ

that visible indication of the positive values of ($\beta > 0$) is that it develops the thermal and velocity boundary-layer thickness while negative values of β show heat absorbers.

Figures 5-7 are sketched for temperature profile. Figure 5(a) plotted temperature profile vs. Prandtl number. Temperature distribution reduces as the Prandtl number becomes pronounced. Particularly, Prandtl number $Pr = 0.72, 1$ and 0.7 corresponding to air and electrolyte solutions, etc. But here we have selected arbitrarily as ($Pr \geq 1$). The physical reason behind this phenomenon is that greater value of relatively lower thermal conductivity and as consequence reduction in thermal boundary-layer thickness and a decrement in the heat transfer rate over the boundary surface which causes to decrease temperature profile significantly. Variation of Eckert number on temperature distribution can be viewed in fig. 5(b). Figure 5(b) demonstrates that temperature enhances as Eckert number increases. According to the definition of it is directly proportional to square of velocity $\bar{u}_w(x)^2$. Hence, an increase in the stretching rate of the sheet for higher values of Eckert number and thus a large enhancement through the motion of fluid particles adjacent to the surface, which causes increment in the temperature of the fluid, particularly in the vicinity of the sheet. Figures 6(a) and 6(b) are displayed for suction/injection parameter. From both the figures it is monitored that when the suction/injection parameter increases

Table 2. Numerical values of Nu for different values of M, K, Pr, and Ec for shrinking case ($\alpha < 0$)

| Ec | Pr | M | K | $Nu_x/Re_x^{1/2}$ |
|-----|-----|-----|-----|-------------------|
| 0.1 | 1 | | | 1.0833 |
| 0.4 | | | | 0.9646 |
| 0.7 | | | | 0.8547 |
| | 1.0 | | | 0.9271 |
| | 2.0 | | | 1.1949 |
| | 3.0 | | | 1.3921 |
| | | 0.4 | | 0.8989 |
| | | 1.0 | | 1.0554 |
| | | 1.5 | | 1.1679 |
| | | | 0.5 | 0.9509 |
| | | | 1.5 | 0.9840 |
| | | | 2.5 | 1.0540 |

($\beta > 0$) or decreases ($\beta < 0$), the temperature profile enhances. Physically, the case ($\beta > 0$) in the boundary-layer bring forth energy which causes the temperature of the fluid to enhance. In most of the cases the presence of heat suction *i. e.* ($\beta < 0$), in the boundary-layer, assimilates energy which results from the reduction in temperature. Figure 7 shows that temperature profile increases for higher values of Hartman parameter. The magnetic parameter causes retardation in the velocity of the flow which has been discussed in fig. 3(a).

Conclusion

In this article, Heat transfer analysis of MHD stagnation point flow over a permeable shrinking/stretching sheet through a pervious media has been examined numerically. The governing equations have been reduced to the ordinary differential equation by utilizing similarity variables. The resulting coupled non-linear ordinary differential equations have been solved by employing SLM and CSC method. Numerical comparison with the preceding published articles bears witness that the current outcomes are in good agreement. Following points are concluded.

- It is noted that by enhancing the magnetic field, M , and porosity parameter, K , boosts the velocity of the fluid.
- It is also recorded that for taking high values in the Prandtl number, Pr , decreases the temperature distribution decreases when increases while its behavior is opposite for Eckert number, Ec .

Nomenclature

| | | | |
|--------------------|---|----------------------|---|
| a, b | – constans | <i>Greek symbols</i> | |
| B_0 | – magnetic field, [Wbm^{-2}] | $\bar{\alpha}$ | – thermal conductivity of the fluid, [$Wm^{-1}K^{-1}$] |
| c_p | – specific heat at constant temperature, [$Jkg^{-1}K^{-1}$] | α | – stretching/shrinking parameter |
| Ec | – Eckert number | β | – suction/injection parameter |
| K | – dimensionless porosity parameter | $\bar{\gamma}$ | – reaction rate of solute |
| \bar{k} | – porosity parameter | θ | – dimensionless temperature |
| M | – Hartmann number | κ | – thermal conductivity, [$Wm^{-1}K^{-1}$] |
| Pr | – Prandtl number | μ | – viscosity of the fluid, [$kgm^{-1}s^{-1}$] |
| p | – pressure, [Nm^{-2}] | ν | – kinematic viscosity, [$kgm^{-1}s^{-1}$] |
| Re_x | – local Reynolds number | ρ | – density of the fluid, [kgm^{-3}] |
| \bar{T} | – fluid temperature, [K] | σ | – electrical conductivity of the fluid, [$\Omega^{-1}m^{-1}$] |
| \bar{u}, \bar{v} | – velocity components, [ms^{-1}] | Ω | – dimensionless temperature difference |
| x, y | – Cartesian coo-ordinate, [m] | | |

Reference

- [1] Hiemenz, K., Die grenzschicht an einem in den gleichformigen flussigkeitsstrom einge tauchten geraden kreiszylinder (in German), *Dinglers Polytech. J.*, 326 (1911), pp. 321-324
- [2] Crane, L. J., Flow Past a Stretching Plate, *Zeitschrift für angewandte Mathematik und Physik ZAMP*, 21 (1970), 4, pp. 645-647
- [3] Paultet, J., Weidman, P., Analysis of Stagnation Point Flow Toward a Stretching Sheet, *International Journal of Non-Linear Mechanics*, 42 (2007), 9, pp. 1084-1091
- [4] Bhattacharyya, K., et al., Slip Effects on Boundary-Layer Stagnation-Point Flow and Heat Transfer Towards a Shrinking Sheet, *International Journal of Heat and Mass Transfer*, 54 (2011), 1-3, pp. 308-313
- [5] Das, K., Slip Effects on MHD Mixed Convection Stagnation Point Flow of a Micropolar Fluid Towards a Svertical Sheet, *Computers and Mathematics with Applications*, 63 (2012), 1, pp. 255-267
- [6] Akbar, N. S., et al., Numerical Analysis of Magnetic Field Effects on Eyring-Powell Fluid-Flow Towards a Stretching Sheet, *Journal of Magnetism and Magnetic Materials*, 382 (2015), May, pp. 355-358

- [7] Majeed, A., et al., Unsteady Ferromagnetic Liquid-Flow and Heat Transfer Analysis over a Stretching Sheet with the Effect of Dipole and Prescribed Heat Flux, *Journal of Molecular Liquids*, 223 (2016), Nov., pp. 528-533
- [8] Shahid, A., et al., Numerical Study of Radiative Maxwell Viscoelastic Magnetized Flow from a Stretching Permeable Sheet with the Cattaneo-Christov Heat Flux Model, *Neural Computing and Applications*, 30 (2017), 11, pp. 1-12
- [9] Bhatti, M. M., Rashidi, M. M., Numerical Simulation of Entropy Generation on MHD Nanofluid Towards a Stagnation Point Flow over a Stretching Surface, *International Journal of Applied and Computational Mathematics*, 3 (2017), 3, pp. 2275-2289
- [10] Rosali, H., M. M., The Effect of Unsteadiness on Mixed Convection Boundary-Layer Stagnation-Point Flow over a Vertical Flat Surface Embedded in a Porous Medium, *International Journal of Heat and Mass Transfer*, 77 (2014), Oct., pp. 147-156
- [11] Rosali, H., et al., Stagnation Point Flow and Heat Transfer over a Stretching/Shrinking Sheet in a Porous Medium, *International Communications in Heat and Mass Transfer*, 38 (2011), 8, pp. 1029-1032
- [12] Rashidi, M. M., et al., Free Convective Heat and Mass Transfer for MHD Fluid-Flow over a Permeable Vertical Stretching Sheet in the Presence of the Radiation and Buoyancy Effects, *Ain Shams Engineering Journal*, 5 (2014), 3, pp. 901-912
- [13] Prasannakumara, B. C., et al., Effects of Chemical Reaction and Non-Linear Thermal Radiation on Williamson Nanofluid Slip Flow over a Stretching Sheet Embedded in a Porous Medium, *Journal of Aerospace Engineering*, 29 (2016), 5, 04016019
- [14] Ghadikolaei, S. S., et al., Boundary-Layer Analysis of Micropolar Dusty Fluid with TiO₂ Nanoparticles in a Porous Medium under the Effect of Magnetic Field and Thermal Radiation over a Stretching Sheet, *Journal of Molecular Liquids*, 244 (2017), Oct., pp. 374-389
- [15] Subhas, A., Veena, P., Visco-Elastic Fluid-Flow and Heat Transfer in a Porous Medium over a Stretching Sheet, *International Journal of Non-Linear Mechanics*, 33 (1998), 3, pp. 531-540
- [16] Eid, M. R., Mahny, K. L., Flow and Heat Transfer in a Porous Medium Saturated with a Sisko Nanofluid over a Non-Linearly Stretching Sheet with Heat Generation/Absorption, *Heat TransferAsian Research*, 47 (2018),1, pp. 54-71
- [17] El-Aziz, M. A., Dual Solutions in Hydromagnetic Stagnation Point Flow and Heat Transfer Towards a Stretching/Shrinking Sheet with Non-Uniform Heat Source/Sink and Variable Surface Heat Flux, *Journal of the Egyptian Mathematical Society*, 24 (2016), 3, pp. 479-486
- [18] Mabood, F., et al., The MHD Stagnation Point Flow and Heat Transfer Impinging on Stretching Sheet with Chemical Reaction and Transpiration, *Chemical Engineering Journal*, 273 (2015), Mar., pp. 430-437
- [19] Hayat, T., et al., The MHD Flow and Heat Transfer over Permeable Stretching Sheet with Slip Conditions, *International Journal for Numerical Methods in Fluids*, 66 (2011), 8, pp. 963-975
- [20] Aman, F., et al., Magnetohydrodynamic Stagnation-Point Flow Towards a Stretching/Shrinking Sheet with Slip Effects, *International Communications in Heat and Mass Transfer*, 47 (2013), Oct., pp. 68-72
- [21] Yasin, M. H. M., et al., The Mhd Stagnation-Point Flow and Heat Transfer with Effects of Viscous Dissipation, Joule Heating and Partial, Velocity Slip, *Scientific Reports*, 5 (2015), Dec., p. 17848
- [22] Bhatti, M. M., Rashidi, M. M., Entropy Generation with Non-Linear Thermal Radiation in MHD Boundary-Layer Flow over a Permeable Shrinking/Stretching Sheet: Numerical Solution, *Journal of Nanofluids*, 5 (2016), 4, pp. 543-548
- [23] Bhatti, M. M., et al., Numerical Study of Entropy Generation with Non-Linear Thermal Radiation on Magnetohydrodynamics Non-Newtonian Nanofluid through a Porous Shrinking Sheet, *Journal of Magnetism*, 21 (2016), 3, pp. 468-475
- [24] Rashidi, M. M., et al., Heat and Mass Transfer Analysis on MHD Blood Flow of Casson Fluid Model Due to Peristaltic Wave, *Thermal Science*, 22 (2018), 6A, pp. 2439-2448
- [25] Shahid, A., Magnetohydrodynamics Nanofluid-Flow Containing Gyrotactic Microorganisms Propagating over a Stretching Surface by Successive Taylor Series Linearization Method, *Microgravity Science and Technology*, 30 (2018), Mar., pp. 445-455
- [26] Bhatti, M. M., et al., A Robust Numerical Method for Solving Stagnation Point flow over a permeable Shrinking Sheet under the Influence of MHD, *Applied Mathematics and Computation*, 316 (2018), Jan., pp. 381-389
- [27] Bhatti, M. M., et al., Entropy Generation as a Practical Tool of Optimisation for Non-Newtonian Nanofluid-Flow through a Permeable Stretching Surface Using SLM, *Journal of Computational Design and Engineering*, 4, (2017), 1, pp. 21-28

- [28] Wang, C. Y., Stagnation Flow Towards a Shrinking Sheet, *International Journal of Non-Linear Mechanics*, 43 (2008), 5, pp. 377-382
- [29] Mekheimer, K. S., *et al.*, Peristaltically Induced Flow Due to a Surface Acoustic Wavy Moving Wall, *Chinese Journal of Physics*, 51 (2013), 5, pp. 968-982
- [30] Mekheimer, K. S., *et al.*, Peristaltically Induced MHD Slip Flow in a Porous Medium Due to a Surface Acoustic Wavy wall, *Journal of the Egyptian Mathematical Society*, 22 (2014), 1, pp. 143-151